Acta Universitatis Sapientiae
Electrical and Mechanical Engineering, 10 (2018) 90-101

DOI: 10.2478/auseme-2018-0006

Simulating Solid Tumors with a Microenvironment-Coupled Agent-Based Computational Model

Dániel KISS[1], Anna LOVRICS[2]

[1] Doctoral School of Applied Informatics and Applied Mathematics,
Óbuda University, Budapest, e-mail: kiss.daniel@nik.uni-obuda.hu
[2] Institute of Enzymology, Research Centre for Natural Sciences,
Hungarian Academy of Sciences, Budapest, e-mail: anna.lovrics@gmail.com

Manuscript received July 25, 2018; revised December 15, 2018.

Abstract: In this paper, we introduce a three-dimensional lattice-based computational model in which every lattice point can be occupied by an agent of various types (e.g. cancer cell, blood vessel cell or extracellular matrix). The behavior of agents can be associated to different chemical compounds that obey mass-transfer laws such as diffusion and decay in the surrounding environment. Furthermore, agents are also able to produce and consume chemical compounds. After a detailed description, the capabilities of the model are demonstrated by presenting and discussing a simulation of a biological experiment available in the literature.

Keywords: Agent-based model, On-lattice computational model, Tumor growth characteristics, Hypoxia, Necrotic core formation

1. Introduction

Computational modeling of biological processes such as tumor growth or the onset of drug resistance is a widely researched area. These complex mechanisms are usually explained by both intracellular alterations and interactions with the local environment, however, many aspects of these events show nonlinear behavior, which makes laboratory experiments hard to design and perform. Not mentioning the cost aspects, mathematical and computational models can be efficiently used to pre-test hypotheses of different biological phenomena which cannot be carried out in standard laboratory experiments.

Solid tumors of clinically relevant sizes consist billions of cells. Simulating the evolution of such cell conglomerates is computationally challenging, especially if we wish to follow the faith of each cell one by one. Agent-based modeling is a reliable and frequently used technique to simulate the collective behavior of many particle-like individual objects like biological cells.

Nowadays, one may choose either from many *out-of-the-box* simulation frameworks [1–3] or computational models presented in the literature depending on the purpose. It was shown, that agent-based simulations can be efficiently used to study the properties (e.g growth, pattern formation or death) of a relatively low number of agents [4, 5] as well as emergent behavior of epithelial cell cultures [6], just to mention a few possibilities. However, performing simulations with a large number of cells (e.g. simulating a few mm^3 of tissue) is still computationally challenging. To overcome this problem, models can be tailored for high performance computing architectures [7, 8] or can be simplified significantly to be feasible to run on a standard workstation computer [9].

In this paper, an agent-based computational model of cells coupled to differential equations governing the mass transport of chemical compounds, especially designed for workstations and laptop computers is presented. As a trade-off between the size of the simulated space and computational performance, many features of the agents are greatly simplified. The agent-based part of the model as well as the differential equations are described in Sec. 2. The effect of choosing different parameters is presented in Sec. 3A and 3B. To demonstrate the capabilities of the coupled model, the simulation of tumor hypoxia, a process in which cells inside of a tumor spheroid perish due to the lack of oxygen is also presented in Sec. 3C.

2. Model description

A. On-lattice agent-based model

The model is defined on a three-dimensional regular lattice $L \subset \boldsymbol{Z}^3$ on which sites can be occupied by single agents in a similar way as presented in [9]. It was shown, that this approach highly reduces the computation costs of the simulation by ignoring the mechanical characteristics of the agents without losing the relevance of the model.

The basic unit of the model is an *agent* representing a biological cell. Agent i is defined by its position $\mathbf{x}_i \in L$, genotype $\theta_i \in \Theta$, phenotype $\phi_i \in \Phi$, maturity stage $m_i \in \boldsymbol{Z}_0^+$, duplication time $\tau_i \in \boldsymbol{R}^+$, motility $\nu_i \in \boldsymbol{R}_0^+$ and aggressivity $\alpha_i \in [0,1]$.

Position $\mathbf{x}_i$ defines the site which is fully occupied by i, therefore $\mathbf{x}_i(t) \neq \mathbf{x}_j(t)$ when $i \neq j$ for all $t \in [0, T_{\max}]$. Genotype set Θ defines a collection of possible cell types, such as *healthy cell*, *cancer cell* or *blood vessel cell*. Different agent types adhere to different rule sets, for instance it is possible to define rules that only apply to blood vessel cells. Phenotype ϕ_i defines the current behavior of agent i (e.g. the rate of production of a chemical compound).

Grid spacing l_L defines the fineness of the simulated space and it can be directly related to the volume of a biological cell. This parameter also influences the resolution of the microenvironment (see Sec. 2D).

B. Cell motility

Cell movement is modelled by performing motility trials on each cell (see Sect. 2E for more details). Motility ν_i characterizes the ability of agent i to move towards another site of L. A motility trial performed on agent i consists of

(i) calculating a displacement probability

$$p_i = \frac{\nu_i \cdot \Delta t_m}{l_L}, \tag{1}$$

(ii) randomly selecting a neighboring site $\mathbf{x}_i^{\text{new}}$ of i,

(iii) updating $\mathbf{x}_i = \mathbf{x}_i^{\text{new}}$ with probability p_i only if $\mathbf{x}_i^{\text{new}}$ is an empty site.

Hence agent i with no neighboring sites moves with a characteristic velocity ν_i. Conversely, if all neighboring sites of i are occupied then $\mathbf{x}_i$ does not change (i.e. agent i turns into stationary until at least one of its neighboring site becomes vacant).

C. Cell proliferation

Maturity stage m_i and duplication time τ_i is related to a process called *cell proliferation* during which a biological cell replicates itself periodically. This could be modeled as a single-step transition with probability $\Delta t_p/\tau_i$, which correctly reproduces the mean growth rate of the overall population. However, the inter-replication times of i follow an exponential distribution, which is biologically not plausible as it can be seen in Fig. 1.

To make a simple yet reasonable model of cell duplication we use the multistage concept proposed in [11] by splitting the cell cycle into k independent exponentially distributed stages. Then, the time to progress through these stages is exponentially distributed, therefore, if the transition rates between stages are identical, the cumulated progression time is Erlang distributed with scale parameter τ_i/k and shape parameter k. Fig. 1 shows that experimentally observed cell cycle times (the time difference between successful duplications of a cell) can be better described using this concept. By choosing appropriate values for τ and k various cell types can be described accurately.

In the simulations, when agent i finishes the progression through its cell cycle ($m_i = k$) it undergoes a replication trial as described in the next paragraph.

The aggressivity value α_i influences this process by defining the probability of the following scenarios.

(S1) Agent i may replicate into an empty neighboring site with probability $1 - \alpha_i$.

(S2) Agent i replicates unconditionally with probability α_i by determining the direction which belongs to the minimal number of other agents which are needed to be shifted by one site to make an empty site for replication.

During this trial process, i may be copied to a randomly selected neighboring site. If the selected site is empty or becomes empty after a shifting procedure described as (S2), then a duplicate of i is placed into that site, otherwise the trial is repeated after Δt_p simulation time.

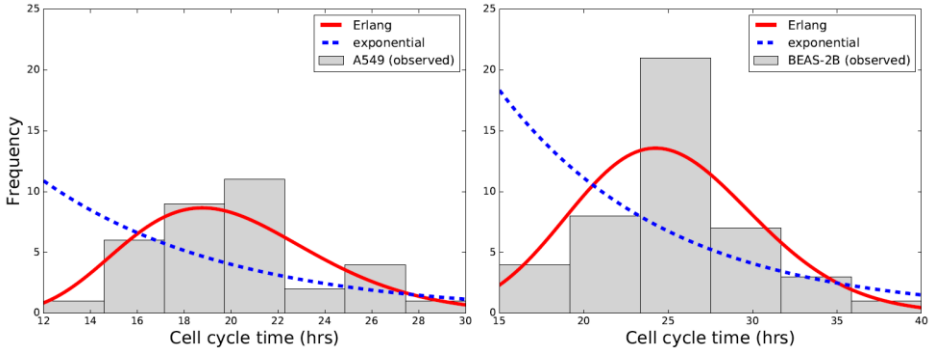

Figure 1: Distribution of experimentally observed duplication times in A549 (left) and BEAS-2B (right) cell cultures reproduced from the data available in [10]. Note the poor agreement between the best-fit exponential distribution ($\lambda_{A549} = \frac{1}{20.1}$ and $\lambda_{\text{BEAS-2B}} = \frac{1}{25.0}$, blue dashed line) and the observed data. Fitting a gamma distribution (or specifically, Erlang distribution, red solid line) describes the data more accurately.

D. Diffusion-decay model

To describe the chemical processes in the environment of biological cells (the so-called *microenvironment*) we numerically solve partial differential equations similar to [12]. Processes including diffusion, decay and concentration modifications caused by agents (e.g. vasculature or agent uptake and secretion) of chemical compound ρ_j are governed by

$$\frac{\partial \rho_j}{\partial t} = \underbrace{D_j \nabla^2 \rho_j - \lambda_j \rho_j}_{\text{diffusion and decay}} + \underbrace{\sum_{\text{agent } i} \mathbf{1}_i(\mathbf{x}) \left[S_j^i \left[\rho_j^* - \rho_j \right] - U_j^i \rho_j \right]}_{\text{agent secretions and uptakes}} \tag{2}$$

on $\Omega \subset \boldsymbol{R}^3$ with no-flux boundary conditions and $\rho_j(\mathbf{x}, t) = f_j$ in Ω. The first term is responsible for the diffusion and the natural decay of compound j, while the second term modifies ρ_j in $\mathbf{x} \in \Omega$ only if $\mathbf{x}$ is overlayed by agent i. Symbol

ρ_j^* denotes the concentration at which compound j saturates. A detailed description of how this PDE model works can be found in [12]. Note, that both coefficients S and U can be chosen arbitrary and independently from i and j, therefore it is possible to define agents that only alter some of the concentrations of compounds in the microenvironment.

E. Time scales and implementation

The simulation of the model is a sequence of calculations and transitions for each $t \in [0, T_{\max}]$. The following time units are used.

(i) Δt: defines the base time step of the simulation. Numerical calculations for mass transport discussed in Sec. 2D are based on Δt. The magnitude of this unit ranges from milliseconds to seconds.

(ii) Δt_m: defines the time step of motility trials. When $t \equiv 0 (\mathrm{mod}\, \Delta t_m)$ a motility trial is performed on all agents as detailed in Sec. 2B. The magnitude of this unit ranges from seconds to minutes.

(iii) Δt_p: defines the time step of proliferation trials. When $t \equiv 0 (\mathrm{mod}\, \Delta t_p)$ a replication trial is performed on all agents that has reached the end of the cell cycle as detailed in Sec. 2C. The magnitude of this unit ranges on a few minutes.

The model was implemented in C# using the standard framework packages. Simulation states were stored regularly on the local disk, and snapshot images were rendered using Mayavi data visualizer [13]. Numerical approximation of the solution was obtained by a finite difference discretization of (2) using a parallelized FTCS explicit method. This generally used scheme provides a good trade-off between accuracy and programming effort [14].

3. Results

A. The effect of motility on growth characteristics

In the absence of chemoattractants or other signals, isolated biological cells have been observed to perform a random walk [15]. This behavior can be easily reproduced by the model detailed in Sec. 2B. However, agent's characteristic velocity v not only influences the movement of the detached agents, but also has an effect on spheroid growth.

Multiple simulations were executed, starting from one agent placed in the center of the simulation space. No chemical compounds were defined, therefore spatially isolated agents did not influence each others' behavior. When an agent

replicated, the descendant inherited all parameter values from its ancestor, hence, the values did not change during the simulation.

Fig. 2 shows representative images of how different values of ν alter the diameter and regularity of a growing spheroid. All relevant parameters of the agents are given in the caption of the figure. As expected, low motility values ($\nu \approx 0$ μmh^{-1}) produce regularly shaped spheroids with sharp surface limits, while high motility ($\nu \gg 0$ μmh^{-1}) results in a more diffuse border and scattered shape. Furthermore, the calculated growth rate of the spheroid also becomes larger due to the increased number of empty sites inside the spheroid.

B. The effect of duplication aggressivity on growth characteristics

Most healthy cells are only able to replicate themselves if there is enough empty space in their surrounding environment. On the contrary, cancer cells are often characterized by the loss of ability to stop proliferation even in a fully occupied environment. To capture this behavior, we introduced the model parameter α which describes the "aggressivity" of an agent during duplication.

When agent i is marked for replication, it randomly selects a strategy depending on α as described in Sec. 2C. By correctly choosing the value of α, it is possible to simulate tumor spheroids growing at different rates, even if the agents have the same τ mean duplication times. Low values of α lead to a power-law-like kinetics, when the diameter of the spheroid grows linearly, hence the number of agents $N \propto t^3$. This is because only agents on the surface of the growing spheroid can replicate due to insufficient space inside.

To test the behavior of our model regarding to parameter α, we started simulations from only one agent, and their parameters were inherited without modification on duplication as described in Sec. 3A.

We found that using high values of the parameter ($\alpha \approx 1$) the number of agents grows exponentially, and newly created agents are distributed uniformly inside the spheroid as it can be seen in Fig. 3. Parameters of the agents as well as their approximate number can be found in the caption of the figure.

C. Microenvironment-coupled state transitions of the agents

We simulated the oxygen consumption of a tumor spheroid grown in an oxygen-rich environment. As it was presented in [16], solid tumors form distinct layers of cells from their surface to inner regions. The limited availability of oxygen causes cell hypoxia followed by necrosis (a type of cell death) in the core of the spheroid. Biological experiments confirmed the relationship between the thickness of the oxygen-rich outer layer called the *viable rim* and the diameter of the tumor spheroid.

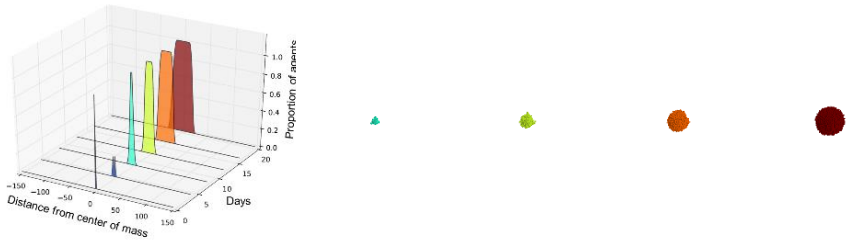

(*a*) Without motility ($\nu = 0$ μmh^{-1}) the growing spheroid forms a dense ball with a well-defined sharp boundary, but the diameter of the spheroid increases slowly because only the agents on the surface are able to duplicate.

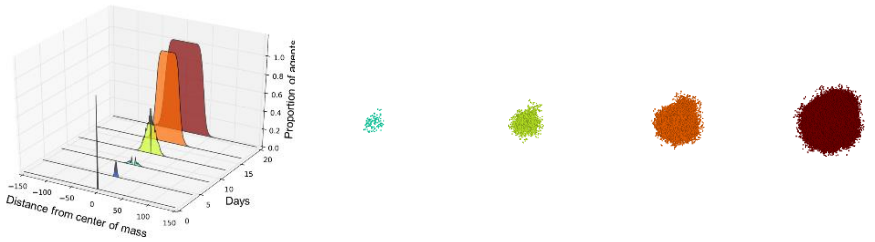

(*b*) With moderate motility ($\nu = 5$ μmh^{-1}) the growth rate of the diameter is clearly increased without the spheroid becoming significantly irregular or scattered. This is mainly because the diameter of the spheroid grows on the same magnitude as the traversable path of the agents via diffusion-like random motion.

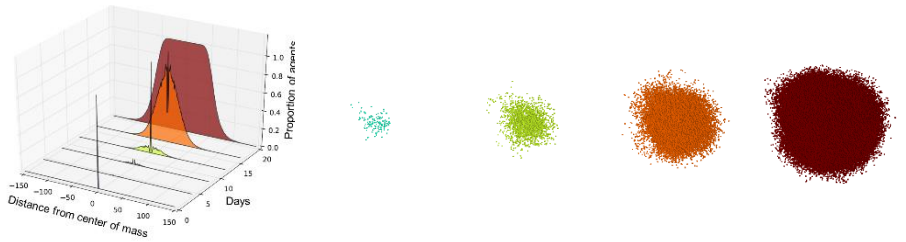

(*c*) High motility ($\nu = 20$ μmh^{-1}) results in a sparse, less regular cluster with scattered border. In this situation, agents are able to travel longer paths between two successive duplication events.

Figure 2: The effect of different values of ν on a growing spheroid started from a single agent. Density diagrams on the left show the proportion of occupied sites at a given distance from the center of mass of the cell cluster. Narrow, continuous, steep-tailed plots belong to dense, regular spheroids. Note, that colors of the spheroids on the right correspond to the density diagram. Parameters used for the simulation: $\tau = 24$ hours, $k = 12$, $\Delta t_p = 15$ min, $\alpha = 0$.

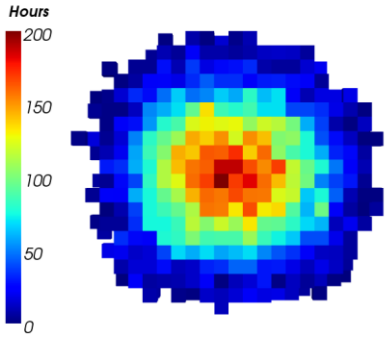

(*a*) Normal duplication strategy ($\alpha = 0$): the duplication process is executed only if a randomly selected neighbor site is empty. Only the agents on the surface of the spheroid are able to perform duplication.

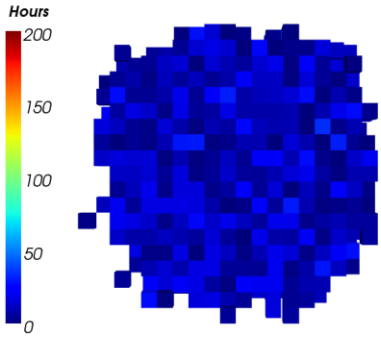

(*b*) Aggressive duplication strategy ($\alpha = 1$): the duplication process is always executed, even if all neighboring sites are occupied. Agents inside the spheroid also duplicate by pushing another agent toward the surface.

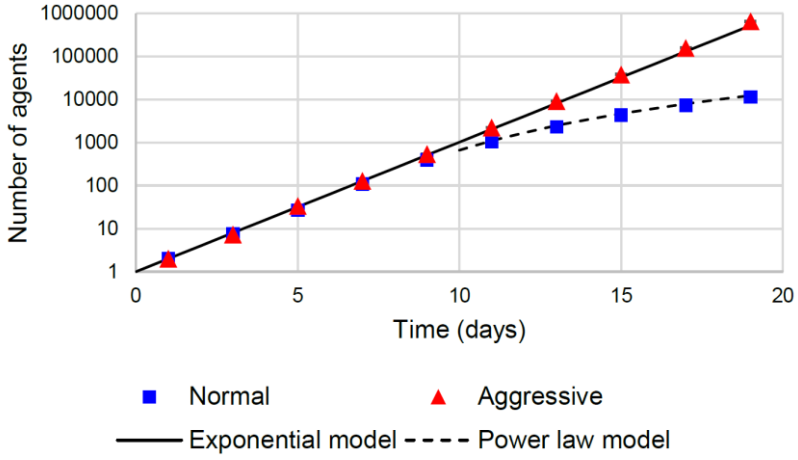

(*c*) Size of simulated tumor spheroids using different duplication strategies. Using $\alpha \approx 0$ an initial exponential phase is followed by a linear phase – i.e., the diameter of the tumor spheroid grows linearly. This phase can be well-described with a power law tumor growth model. When $\alpha \approx 1$ the number of agents in the spheroid keeps growing exponentially even after the initial phase.

Figure 3: Cross-section of the simulated tumor spheroids and their growth curves using different duplication strategies. Simulations were started from one agent and stopped at $T_{\max} = 19$ days. For cross-section images we selected a time point, when approximately 4000 agents were present. Agent colors are related to the time passed since the last duplication event of the agent. Parameters used for the simulation: $\tau = 24$ h, $k = 12$, $\Delta t_p = 15$ min, $\nu = 0$ μmh^{-1}, $\alpha = 0$ and $\alpha = 1$.

First, we generated a two-dimensional circular set of *cell* agents with diameter d, as a model of a slice of the whole tumor spheroid. We assumed that the oxygen concentration in the surrounding environment is constant during the experiment, therefore we marked all non-cell nodes as oxygen sources. This means, that oxygen concentration on these outer grid points was constantly $\rho_{O_2,\text{normal}}$. When an agent is present on a certain grid point, it acts as a sink of oxygen, therefore oxygen concentration reduces according to (2), however, oxygen concentration may also increase due to diffusion from outer regions.

When the oxygen concentration on an inner grid point inside the spheroid falls below $\rho_{O_2,\text{critical}}$ the corresponding cell agent (if the site is occupied) changes its type and becomes *necrotic*. Necrotic type agents are unable to move or duplicate, and the transition is irreversible. As a consequence of these two counter-directional processes – oxygen consumption of agents and diffusion from outer regions – a necrotic region starts to grow in the core of the spheroid. As the diameter of the spheroid increases, so does the necrotic region, but the thickness of the viable rim decreases, just as it was observed in real experiments.

Multiple simulations were executed with the same parameter set to average stochastic effects. Results of each simulation were evaluated by

(i) determining the convex hull of both the whole spheroid (H_0) and the necrotic region (H_n) at a given time,

(ii) calculating the mean distance r_0 and r_n between the mass of center of the spheroid and the points in H_0 and H_n, respectively,

(iii) calculating the viable rim thickness as $r_c = r_0 - r_n$.

We found a qualitative accordance with the model presented in [16], meaning that the viable rim thickness decreases as the diameter of the spheroid increases (see quantitative results in Fig. 4c). The exact parameter values of the agents as well as the relevant coefficients of the mass-transport model can be found in the caption of the figure.

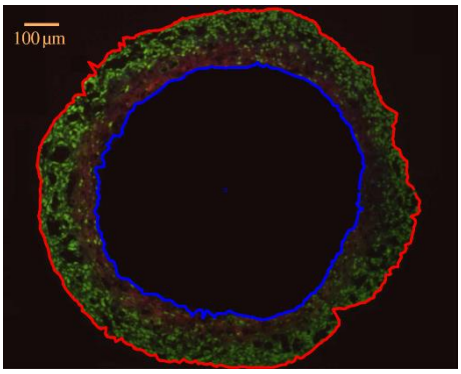

(*a*) Image of a tumor spheroid cross-section. Proliferating (living) cells are shown as green particles near the spheroid boundary marked by a red line. The hypoxic core boundary is shown by the blue line. (Photo by Grimes et al. [16] licensed under the terms of Creative Commons Attribution License.)

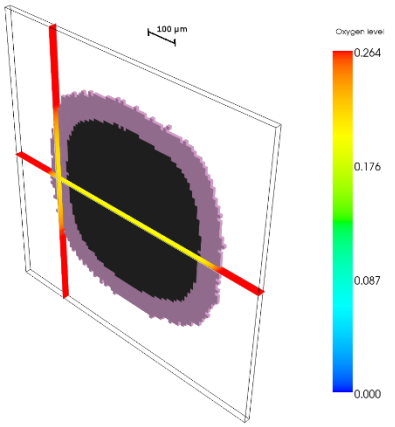

(*b*) Representative image of a simulation. Pink dots represent living agents, black dots show necrotic (dead) agents. Note the color-scaled section planes showing oxygen concentration of the microenvironment.

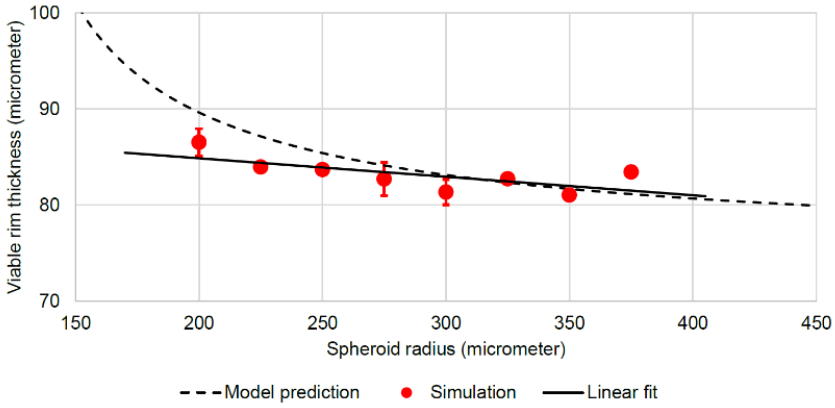

(*c*) The thickness of the viable rim of a tumor spheroid depends on its radius. The dashed line shows the predicted value of the viable rim using the model of Grimes et al. with $r_l = 130$ µm. In agreement with the prediction the best linear fit of simulation data shows a clear decreasing tendency as the spheroid diameter grows. Simulation data shows mean±SD.

Figure 4: The effect of oxygen consumption of cells in a tumor spheroid. Low oxygen level leads to necrosis in the core of a growing spheroid. Parameters used for the simulation: $\tau = 24$ h, $k = 12$, $\Delta t_p = 15$ min, $\nu = 0$ µmh^{-1}, $\alpha = 0$. In (2) we set $\rho_{O2,normal} = 0.264$, $\rho_{O2,critical} = 0.2$, $D_{O_2} = 6 \times 10^{-8}$m^{2}h^{-1}, $U_{O_2}^{cancercell} = 0.1$ min^{-1}, $\lambda_{O_2} = 0.01\, U_{O_2}^{cancercell}$ and $\Delta t = 500$ ms according to literature data [17].

4. Conclusion

This paper presented an on-lattice computational model of solid tumors in which individual units (so-called agents) are coupled to their microenvironment. Features of agents like motility, proliferation potential or sensitivity to different compounds from the microenvironment can be set independently. The simplicity of the model makes it possible to simulate a few mm^3 of tissue on a standard desktop workstation or laptop computer, in reasonable time.

The effects of different values of agents' motility and aggressivity parameters were tested along with their microenvironment-coupled behavior. In agreement with experimental observations we found that both the motility and the aggressive proliferation influences the size and the shape of a growing solid tumor. It is also have to be mentioned, that high motility or aggressive duplication strategy of the agents makes the simulation slightly slower, especially for large and dense clusters. This effect could be compensated by a selection heuristic we recently presented for an off-lattice agent based model [18].

Simulation results of the development of a well-oxygenated viable rim in tumor spheroids show good qualitative match to real biological observations, however, optimal parameters of the model must be determined to achieve quantitative match as well.

We think that this computational model can be a suitable tool for scientists to give valuable insights into emergent behavior of complex biological systems.

Supplementary information

Additional data including source codes, simulation data and animations are available at https://bitbucket.org/kissdanieldezso/onlatticets.

Acknowledgements

Dániel Kiss was supported by the ÚNKP-17-3/I New National Excellence Program of the Ministry of Human Capacities. Anna Lovrics was supported by OTKA PD124467 grant. The authors wish to thank Gergely Szakács and the members of Membrane Proteins Research Group for their contribution to this project.

References

[1] Starruß, J., de Back, W., Brusch, L., Deutsch, A. "Morpheus: a user-friendly modeling environment for multiscale and multicellular systems biology", *Bioinformatics* 30, 9 (2014) 1331–1332.

[2] Ghaffarizadeh, A., Heiland, R., Friedman, S. H., Mumenthaler, S. M., Macklin, P., "PhysiCell: an open source physics-based cell simulator for 3-D multicellular systems", *PLoS Comput. Biol.* 14, 2 (2018).

[3] Kang, S., Kahan, S., McDermott, J., Flann, N., Shmulevich, I., "Biocellion: accelerating computer simulation of multicellular biological system models", *Bioinformatics* 30, 21 (2014) 3101–3108.

[4] Drasdo, D., Höhme, S., "Individual-Based Approaches to Birth and Death in Avascular Tumors", *Mathematical and Computer Modelling* 37, (2003) 1163–1175.

[5] Drasdo, D., Hoehme, S., Block, M., "On the Role of Physics in the Growth and Pattern Formation of Multi-Cellular Systems: What can we Learn from Individual-Cell Based Models?", *Journal of Statistical Physics* 128, 1 (2007) 287–345.

[6] Walker, D. C., Southgate, J., Hill, G., Holcombe, M., Hosea, D. R., Wood, S. M., Mac Neil, S., Smallwood, R. H., "The epitheliome: agent-based modelling of the social behaviour of cells.", *BioSystems* 76, (2004) 89–100.

[7] Cytowski, M., Szymanska, Z., "Large-Scale Parallel Simulations of 3D Cell Colony Dynamics", *Computing in Science & Engineering* 16, 5 (2014) 86–95.

[8] Cytowski, M., Szymanska, Z., Uminski, P., Andrejczuk, G., Raszkowski K., "Implementation of an Agent-Based Parallel Tissue Modelling Framework for the Intel MIC Architecture", *Scientific Programming* 8721612, (2017).

[9] Waclaw, B., Bozic, I., Pittman, M. E., Hruban, R. H., Vogelstein, B., Nowak, M. A., "A spatial model predicts that dispersal and cell turnover limit intratumour heterogeneity", *Nature* 525, 7568 (2015) 261–264.

[10] Summers, H. D., Wills, J. W., Brown, M. R., Rees, P., "Poisson-Event-Based Analysis of Cell Proliferation", *Cytometry A.* 87, 5 (2015) 385–392.

[11] Yates, C. A., Ford, M. J., Mort, R. L., "A Multi-Stage Representation of Cell Proliferation as a Markov Process", *Bulletin of Mathematical Biology* 79, 12 (2017) 2905–2928.

[12] Ghaffarizadeh, A., Friedman, S. H., Macklin, P., "BioFVM: an efficient, parallelized diffusive transport solver for 3-D biological simulations", *Bioinformatics* 32, 8 (2016) 1256–1258.

[13] Ramachandran, P., Varoquaux, G., "Mayavi: 3D Visualization of Scientific Data", *IEEE Computing in Science & Engineering*, 13, 2 (2011), 40–51.

[14] Roberts, D. L., Selim, M. S., "Comparative study of six explicit and two implicit finite difference schemes for solving one-dimensional parabolic partial differential equations", *International Journal for Numerical Methods in Engineering* 20 (1984) 817–844.

[15] Mombach, J., Glazier, J., "Single cell motion in aggregates of embryonic cells", *Phys. Rev. Lett.* 76, 3032 (1996).

[16] Grimes, D. R., Kelly, C., Bloch, K., Partridge, M., "A method for estimating the oxygen consumption rate in multicellular tumour spheroids", *J. R. Soc. Interface* 11, 20131124 (2014).

[17] Macklin, P., Edgerton, M. E., Thompson, A. M., Cristini, V., "Patient-calibrated agent-based modelling of ductal carcinoma in situ (DCIS): From microscopic measurements to macroscopic predictions of clinical progression", *Journal of Theoretical Biology* 301 (2012) 122–140.

[18] Kiss, D., Lovrics, A., "Performance analysis of a computational off-lattice tumor growth model", *Proceedings of the IEEE 30th Jubilee Neumann Colloquium* (2017).